Clim. Past Discuss., https://doi.org/10.5194/cp-2017-151
Manuscript under review for journal Clim. Past
Discussion started: 20 November 2017

Climate of the Past Discussions
Open Access
EGU

Thermocline state change in the Eastern Equatorial Pacific during the late Pliocene/early Pleistocene intensification of Northern Hemisphere Glaciation

Kim A. Jakob[1], Jörg Pross[1], Christian Scholz[1], Jens Fiebig[2], Oliver Friedrich[1]

[1]Institute of Earth Sciences, Heidelberg University, Heidelberg, 69120, Germany
[2]Institute of Geosciences, Goethe-University Frankfurt, Frankfurt, 60438, Germany

Correspondence to: Kim A. Jakob (kim.jakob@geow.uni-heidelberg.de)

Abstract. The late Pliocene/early Pleistocene intensification of Northern Hemisphere Glaciation (iNHG) ~2.5 million years ago (Marine Isotope Stages [MIS] 100–96) stands out as the most recent major tipping point in Earth's climate history. It strongly influenced oceanographic and climatic patterns including trade-wind and upwelling strength in the Eastern Equatorial Pacific (EEP). The thermocline depth in the EEP, in turn, plays a pivotal role in the evolution of short-term climate phenomena such the El Niño-Southern Oscillation, and thus bears important consequences for the Earth's climate system. However, thermocline dynamics in the EEP during to the iNHG have yet remained unclear. While numerous studies have suggested a link between a thermocline shoaling in the EEP and Northern Hemisphere ice growth, other studies have indicated a stable thermocline depth during iNHG, thereby excluding a causal relationship between thermocline dynamics and ice-sheet growth. In light of these contradictory views, we have generated geochemical (planktic foraminiferal $\delta^{18}O$, $\delta^{13}C$ and Mg/Ca), sedimentological (sand-accumulation rates) and faunal (abundance data of thermocline-dwelling foraminifera) records for Ocean Drilling Program Site 849 located in the central part of the EEP. Our records span the interval from ~2.75 to 2.4 Ma (MIS G7–95), which is critical for understanding thermocline dynamics during the final phase of the iNHG. They document a thermocline shoaling from ~2.64 to 2.55 Ma (MIS G2–101) and a relatively shallow thermocline from ~2.55 Ma onwards (MIS 101–95). This indicates a state change in EEP thermocline depth shortly before the final phase of iNHG. Ultimately, our data support the hypothesis that (sub-)tropical thermocline shoaling may have contributed to the development of large Northern Hemisphere ice sheets.

1 Introduction

The onset and intensification of Northern Hemisphere Glaciation during the late Pliocene and early Pleistocene (~3.6–2.4 Ma [Mudelsee and Raymo, 2005]) is part of a long-term cooling trend following the Mid-Piacenzian warm period. The glacial corresponding to Marine Isotope Stage (MIS) G6 (~2.7 Ma) is often considered to mark the onset of large-scale glaciation in the Northern Hemisphere because it is characterized by the first occurrence of ice-rafted debris in the North Atlantic Ocean (Bartoli et al., 2006; Bailey et al., 2013). The first culmination in Northern Hemisphere ice build-up occurred

Clim. Past Discuss., https://doi.org/10.5194/cp-2017-151
Manuscript under review for journal Clim. Past
Discussion started: 20 November 2017

at ~2.5 Ma as documented by the first three large-amplitude (~1 ‰ in the benthic $\delta^{18}O$ record) glacial-interglacial cycles (MIS 100–96) that indicate substantial waxing and waning of ice sheets (Lisiecki and Raymo, 2005). At that time, ice rafting became widespread across the North Atlantic Ocean (Shackleton et al., 1984; Naafs et al., 2013). This so-called "intensification of Northern Hemisphere Glaciation" (iNHG) represents the most recent major tipping point in Earth's climate history. It strongly influenced oceanographic and climatic patterns worldwide, affecting, for example, the amount of biological production in the Eastern Equatorial Pacific Ocean (EEP) (Etourneau et al., 2010; Jakob et al., 2016) – a region that exerts a strong influence on the Earth's climate system through its effects on the global carbon and nutrient cycles (e.g., Schlitzer, 2004; Takahashi et al., 2009).

Today, the shallow depth of the thermocline in the EEP plays a pivotal role in the evolution of short-term climate phenomena including the El Niño-Southern Oscillation (Fedorov et al., 2004; Ma et al., 2013). Its position in the water column thus bears important consequences for the Earth's climate system. In general, proxy records and modeling results consistently document a long-term shoaling of the thermocline in the EEP and other (sub-)tropical upwelling regions throughout the Plio-Pleistocene (Wara et al., 2005; Fedorov et al., 2006; Dekens et al., 2007; Steph et al., 2010; Ford et al., 2012). However, the dynamics of the thermocline in the EEP and its potential links to the iNHG have yet remained enigmatic. Some studies have inferred that thermocline depth reached a critical threshold at ~3 Ma, which allowed trade winds to deliver cool waters from below the thermocline to the surface in (sub-)tropical upwelling regions such as the EEP (Fedorov et al., 2006; Dekens et al., 2007). The timing led to the hypothesis that thermocline shoaling and the development of the "EEP cold tongue" (Wyrtki, 1981) was a necessary precondition for iNHG via a strengthening of the tropical Pacific Walker Circulation and, at the same time, a reduction of poleward heat transport (Cane and Molnar, 2001). Other studies, however, identified fundamental shifts in thermocline depth only prior to ~3.5 Ma (Wara et al., 2005; Steph et al., 2010; Ford et al., 2012), which would imply that thermocline depth in the EEP did not play an important role in the development of large-scale glaciation in the Northern Hemisphere.

In light of these contradictory views, and to ultimately shed new light on potential links between low-latitude thermocline dynamics and high-latitude ice-sheet build-up, we have investigated thermocline state changes during the iNHG in the EEP by integrating new with previously published proxy records from Ocean Drilling Program (ODP) Site 849 (Fig. 1). We use planktic (both sea-surface- and thermocline-dwelling) foraminiferal geochemical ($\delta^{18}O$, $\delta^{13}C$ and Mg/Ca) proxy records in combination with sedimentological (sand-accumulation rates) and faunal (abundance data of thermocline-dwelling foraminiferal species) information to reconstruct thermocline depth for the final phase of the late Pliocene/early Pleistocene iNHG from ~2.75 to 2.4 Ma (MIS G7–95).

Clim. Past Discuss., https://doi.org/10.5194/cp-2017-151
Manuscript under review for journal Clim. Past
Discussion started: 20 November 2017

2 Study area and study site

2.1 The Eastern Equatorial Pacific

The EEP has considerable relevance for the Earth's atmospheric and marine carbon budget (Toggweiler and Sarmiento, 1985; Takahashi et al., 2009), and at the same time exerts strong control on oceanographic and climatic circulation patterns (Fedorov and Philander, 2000; Pennington et al., 2006). Today, as a part of the tropical Pacific Walker Circulation, westward-blowing trade winds in the EEP induce a year-around upwelling of cold waters from below the thermocline to the surface. This results in a thin, nutrient-enriched and relatively cold (~23 °C [Locarnini et al., 2013]) mixed layer, the so-called "EEP cold tongue" (Wyrtki, 1981) (Fig. 1a). In today's oceans, the EEP upwelling system supports more than 10 % of the global biological production (Pennington et al., 2006). The relatively high primary productivity results in exceptionally high sedimentation rates that amount to up to 3.0 cm kyr^{-1} during the past 5 Myr (Mayer et al., 1992; Mix et al., 1995).

The EEP stands out as an ideal natural laboratory for studying the dynamics of the tropical thermocline: Owing to the shallow depth of the thermocline in the present-day EEP upwelling system (~50 m [Wang et al., 2000]) (Fig. 1b), even small changes in its depth can affect surface-water properties such as temperature or nutrient content that can be ideally reconstructed from sediments underneath the "cold tongue". Thereby, the high sedimentation rates allow for the acquisition of proxy records at high temporal resolution compared to outside the EEP upwelling zone.

2.2 ODP Site 849

To reconstruct changes in thermocline depth in the EEP we focused on sediments from ODP Leg 138 Site 849 (coordinates: 0°11′N, 110°31′W; present-day water depth: 3851 m [Mayer et al., 1992]) (Fig. 1). This site has been selected because of (i) its position within the equatorial "cold tongue" west of the East Pacific Rise in the open ocean that makes it less prone to continental influence compared to sites east of the East Pacific Rise (Mix et al., 1995); (ii) the good preservation of foraminifera (Jakob et al., 2016, 2017) despite the fact that the present-day water depth at Site 849 is close to the lysocline (Adelseck and Anderson, 1978; Berger et al., 1982); and (iii) high sedimentation rates (2.7 cm kyr^{-1} for our study interval [Jakob et al., 2017]) with continuous sedimentation (Mayer et al., 1992).

3 Investigated foraminiferal species

The geochemical and faunal records generated in this study are based on the planktic foraminiferal species *Globigerinoides ruber* (white, sensu stricto), *Globorotalia crassaformis*, *Globorotalia menardii*, and *Globorotalia tumida*. *Globigerinoides ruber* generally inhabits the mixed layer and is therefore typically considered to represent surface-water conditions (Fairbanks et al., 1982; Dekens et al., 2002; Steph et al., 2009, and references therein). The species *G. menardii* and *G. tumida* are found in the EEP at depths of ~25–70 m and ~50–125 m, respectively, typically in intermediate-thermocline waters (Fairbanks et al., 1982; Watkins et al., 1998; Faul et al., 2000). *Globorotalia crassaformis* lives at the bottom of the

Clim. Past Discuss., https://doi.org/10.5194/cp-2017-151
Manuscript under review for journal Clim. Past
Discussion started: 20 November 2017

thermocline (Niebler et al., 1999; Regenberg et al., 2009, Steph et al., 2009, and references therein); although its exact depth habitat in the EEP has remained unclear, information from the (sub-)tropical Atlantic suggest that this species is typically found between 500 and 1000 m water depth (Steph et al., 2006; Regenberg et al., 2009, Steph et al., 2009, and references therein; Cléroux et al., 2013; Wejnert et al., 2013). The presumed calcification depths of these species in the EEP are compiled in Fig. 1b.

4 Material and methods

4.1 Sample material

To obtain geochemical, faunal and sedimentological information for Site 849, 374 samples have been investigated along the primary shipboard splice (Mayer et al., 1992) from cores 849C-7H-1-80 cm to 849C-7H-2-21 cm and 849D-6H-5-102 cm to 849D-7H-5-57 cm (77.02–67.78 m composite depth [mcd]). Based on the age model of Jakob et al. (2017), this interval spans from ~2.75 to 2.4 Ma (MIS G7–95). Samples with a volume of 20 cm^3 were investigated at 2 cm intervals, which yields a temporal resolution of ~750 yr. The sample material was dried, weighed, and washed over a 63 µm sieve.

Foraminiferal geochemical records ($\delta^{18}O$, $\delta^{13}C$ and Mg/Ca) of the deep-thermocline-dwelling species *G. crassaformis* and the surface-dwelling species *G. ruber*, as well as sand-accumulation rates were generated from the full sample set (temporal resolution: ~750 yr). From these measurements surface-to-thermocline $\delta^{18}O$, $\delta^{13}C$ and Mg/Ca gradients were calculated. Abundance counts of both deep-thermocline- (*G. crassaformis*) and intermediate-thermocline-dwelling species (*G. menardii* and *G. tumida*) were conducted every 20 cm (temporal resolution: ~7.5 kyr).

For *G. crassaformis*, we have generated new $\delta^{18}O$, $\delta^{13}C$ and Mg/Ca records, except for the interval from ~2.65 to 2.4 Ma for which $\delta^{13}C$ values have already been published by Jakob et al. (2016). For this purpose, an average of 15 individuals per sample was picked from the 315–400 µm fraction. Tests for $\delta^{18}O$ and Mg/Ca analyses were cracked, homogenized and split into two subsamples. For *G. crassaformis*, both sinistral- and dextral-coiling specimens occur at Site 849; geochemical data were preferentially measured on tests with the most abundant coiling direction (sinistral). Sinistral-coiling specimens, however, do not occur continuously across our study interval. Thus, dextral-coiling tests were used for some intervals (in particular from ~2.46 to 2.43 Ma [69.84–69.04 mcd] and from ~2.51 to 2.50 Ma [70.85–70.68 mcd]). Measurements of geochemical parameters ($\delta^{13}C$, $\delta^{18}O$, Mg/Ca) separately on sinistral- and dextral-coiling specimens from the same samples have demonstrated that the reconstructed values are independent of the coiling directions (see also Jakob et al. [2016]).

The number of *G. crassaformis* individuals in the investigated size fraction (315–400 µm), was, however, too low to allow for geochemical analyses in specific intervals. These intervals are from 2.68 to 2.65 Ma (75.39–74.65 mcd corresponding to MIS G3) and from 2.73 to 2.69 Ma (77.02–75.79 mcd corresponding to MIS G7–G5). We decided not to fill these gaps by using another size fraction because (i) this might have biased our Mg/Ca and stable-isotope records due to ontogenetic effects (Elderfield et al., 2002; Friedrich et al., 2012), and (ii) the abundance of *G. crassaformis* specimens <315

Clim. Past Discuss., https://doi.org/10.5194/cp-2017-151
Manuscript under review for journal Clim. Past
Discussion started: 20 November 2017

µm was too low for geochemical analyses in most of the samples where the 315–400 µm *G. crassaformis* size fraction is absent (see Sect. 5.4.2 for details).

For *G. ruber*, the previously published Mg/Ca-based SST and $\delta^{18}O$ datasets of Jakob et al. (2017) were augmented by $\delta^{13}C$ data, except for the interval from ~2.65 to 2.4 Ma for which $\delta^{13}C$ values have already been published by Jakob et al. (2016). For this purpose, an average of twelve specimens was picked from the 250–315 µm size fraction. An overview of all geochemical datasets evaluated in this study is presented in Table 1.

4.2 Analytical methods

4.2.1 Foraminiferal preservation

The preservation of planktic foraminiferal (*G. crassaformis* and *G. ruber*) tests used for geochemical analyses was examined by Scanning Electron Microscope (SEM) images of selected specimens from both glacial and interglacial intervals. Close-up views were taken using a LEO 440 SEM at the Institute of Earth Sciences, Heidelberg University.

4.2.2 Stable-isotope analyses

Oxygen and carbon isotopes of *G. ruber* and *G. crassaformis* were analyzed using a ThermoFinnigan MAT253 gas-source mass spectrometer equipped with a Gas Bench II at the Institute of Geosciences, Goethe-University Frankfurt. Values are reported relative to the Vienna Pee Dee Belemnite (VPDB) standard through the analysis of an in-house standard calibrated to NBS-19. The precision of the $\delta^{18}O$ and $\delta^{13}C$ analyses is better than 0.08 ‰ and 0.06 ‰ (at 1σ level), respectively. $\delta^{13}C$ values of *G. ruber* reported herein have been adjusted for species-specific offset from equilibrium precipitation by the addition of + 0.94 ‰ (Spero et al., 2003), while measured $\delta^{18}O$ values of *G. ruber* have been considered to approximate equilibrium precipitation (Koutavas and Lynch-Stieglitz, 2003) and therefore were not adjusted. For *G. crassaformis* we report the values measured on this species because laboratory investigations on $\delta^{13}C$ and $\delta^{18}O$ fractionation for *G. crassaformis* are still lacking.

4.2.3 Mg/Ca analyses

Samples for Mg/Ca analyses of *G. crassaformis* were carefully cleaned to remove clay minerals, organic material and re-adsorbed contaminants following the protocol of Barker et al. (2003). Analyses were carried out with an Agilent Inductively Coupled Plasma-Optical Emission Spectrometer 720 at the Institute of Earth Sciences, Heidelberg University. Reported Mg/Ca values were normalized relative to the ECRM 752-1 standard reference value of 3.762 mmol/mol (Greaves et al., 2008). To ensure instrumental precision, an internal consistency standard was monitored at least every 20 samples. Based on replicate measurements, a standard deviation for Mg/Ca of ± 0.02 mmol/mol (corresponding to ± 0.12 °C) is obtained. To identify possible contamination by clay particles or diagenetic coatings that might affect foraminiferal Mg/Ca ratios (Barker et al., 2003), elemental ratios of Al/Ca, Fe/Ca and Mn/Ca were screened (see Sect. 5.2).

Clim. Past Discuss., https://doi.org/10.5194/cp-2017-151
Manuscript under review for journal Clim. Past
Discussion started: 20 November 2017

4.2.4 Paleotemperature reconstruction

Species-specific conversions of Mg/Ca to temperature for *G. crassaformis* have only been calibrated based on samples from the Atlantic Ocean (Anand et al., 2003; Regenberg et al., 2009; Cléroux et al., 2013). These equations yield the same trend and amplitudes when applied to *G. crassaformis* Mg/Ca values from Site 849, but differ with regard to absolute values (Fig. 2). We converted Mg/Ca ratios of *G. crassaformis* into temperature following the species-specific equation of Cléroux et al. (2013) for two reasons: (i) The selected calibration is based on specimens with a grain size of 355–425 µm, which matches the size fraction used in our study (315–400 µm) better than the other equations that are available; and (ii) the Mg/Ca range of *G. crassaformis* from Site 849 (~1–3 mmol/mol) fits best to the calibration range (~1–2 mmol/mol) of the equation of Cléroux et al. (2013) compared to the other equations.

Because the equation of Cléroux et al. (2013) is based on oxidative and reductive cleaning of foraminiferal tests, while only oxidative cleaning has been applied to Site 849 samples, measured Mg/Ca values had to be reduced by 10 % (Barker et al., 2003). The pooled uncertainty in the temperature record (analytical error of ± 0.02 mmol/mol [corresponding to ± 0.12 °C] and calibrational error of ± 0.82 °C [Cléroux et al., 2013]) is ± 0.94 °C.

4.2.5 Abundance counts

Abundance counts of deep-thermocline-dwelling (*G. crassaformis,* both sinistral- and dextral-coiling specimens) and intermediate-thermocline-dwelling (*G. tumida* and *G. menardii*) species (Fig. 1b) were generated on the >250 µm size fraction of Site 849 samples. The >250 µm size fraction was split down to at least 400 individual planktic foraminifera using a microsplitter. Abundance counts were converted to mass-accumulation rates using linear sedimentation rates and dry bulk density data (calculated from high-resolution GRAPE density shipboard measurements [IODP JANUS database; Mayer et al., 1992]) following the methodology described in Jakob et al. (2016).

4.2.6 Sand-accumulation rates

The sand-accumulation rates (SAR) available for the MIS G1–95 (~2.65–2.4 Ma) interval from Site 849 as presented in Jakob et al. (2016) were extended back to MIS G7 (~2.75 Ma) in this study. They were calculated using linear sedimentation rates, dry bulk density data (calculated from high-resolution GRAPE density shipboard measurements [IODP JANUS database; Mayer et al., 1992]), and the portion of the >63 µm sand fraction following the approach described in Jakob et al. (2016).

Clim. Past Discuss., https://doi.org/10.5194/cp-2017-151
Manuscript under review for journal Clim. Past
Discussion started: 20 November 2017

5 Results and discussion

5.1 Foraminiferal test preservation at Site 849

Shipboard investigations on core catchers had originally reported a poor preservation of planktic foraminiferal tests at Site 849 (Mayer et al., 1992). However, these observations do not apply to the samples from our study interval. Instead, SEM images of both glacial and interglacial *G. crassaformis* and *G. ruber* specimens show well-preserved fine features such as delicate spines, pore channels and a layered wall structure, and a lack of secondary calcite on test surfaces (Fig. 3). This indicates that test preservation is consistently sufficient for the acquisition of high-quality geochemical data for both species throughout the study interval. A low planktic foraminiferal fragmentation index at Site 849 further confirms this interpretation (Jakob et al., 2017), indicating that dissolution has not considerably affected foraminiferal tests.

5.2 Assessment of contamination and diagenetic effects on Mg/Ca ratios of *G. crassaformis*

Al/Ca, Fe/Ca and Mn/Ca ratios >0.1 mmol/mol are typically considered to indicate the presence of detrital clay, Fe-rich coatings and Mn-rich overgrowth, respectively, and therefore hint at foraminiferal test contamination that might have biased measured Mg/Ca ratios (Barker et al., 2003). In most of our samples the content of Al was below the detection limit, arguing against the presence of detrital clay. With the exception of few samples, Fe/Ca values also commonly do not exceed the critical value of 0.1 mmol/mol and therefore indicate no contamination by Fe-rich overgrowth (Fig. 4a). The lack of a statistically significant correlation between Mg/Ca and Fe/Ca ratios (r^2 = 0.17, p <0.01) further supports this finding. Measured Mn/Ca ratios, however, were above the 0.1 mmol/mol threshold and therefore might indicate Mn-rich overgrowth on the analyzed tests (Fig. 4b). Our data show a weak correlation between Mg/Ca and Mn/Ca ratios for *G. crassaformis* samples (r^2 = 0.44, p <0.01) that indeed might indicate a bias of measured Mg/Ca ratios due to a Mn-rich overgrowth. We note, however, that SEM images argue against the existence of any kind of overgrowth (Fig. 3).

Diagenetic overgrowth usually has a Mg/Mn ratio of ~0.1 mol/mol (Barker et al., 2003, and references therein). If an unrealistically high Mg/Mn ratio of 1 in the diagenetic overgrowth is assumed, this might change temperature estimates by on average ~0.5 °C; however, we note that this would not affect the overall shape of the Mg/Ca-based temperature record (Fig. 4c, d). Although we cannot completely rule out the possibility of diagenetic changes in the *G. crassaformis* tests because of significantly enriched Mn/Ca ratios, we conclude with reasonable certainty that early diagenetic overprinting (if existing) has no significant impact on the interpretation of our data.

5.3 Stable-isotope and Mg/Ca records of *G. crassaformis* and *G. ruber* at Site 849

In the tropics, where seasonal climate variability is low, geochemical signatures of the investigated foraminiferal species are typically considered not to be seasonally biased (Lin et al., 1997; Tedesco et al., 2007). Therefore, all data presented in this study are inferred to reflect mean annual conditions.

Clim. Past Discuss., https://doi.org/10.5194/cp-2017-151
Manuscript under review for journal Clim. Past
Discussion started: 20 November 2017

The $\delta^{18}O$ record of *G. crassaformis* varies between 0.91 ‰ and 2.79 ‰ throughout the study interval (~2.75–2.4 Ma) (Fig. 5b). Lowest values correspond to interglacials and highest values are associated with glacials. With a mean value of 2.01 ‰, $\delta^{18}O$ values of *G. crassaformis* (this study) are on average 2.78 ‰ higher than those of *G. ruber* (Jakob et al., 2017), indicating cooler and/or more saline waters in the depth habitat of *G. crassaformis* (bottom of the thermocline) compared to *G. ruber* (surface waters) (Fig. 1b; see Sect. 3 for details). In theory, a deeper depth habitat of *G. crassaformis* than of *G. ruber* should result in a lower $\delta^{13}C$ signature in *G. crassaformis* tests than in those from *G. ruber* since the amount of organic matter remineralization and the associated release of light ^{12}C into the surrounding water typically increases with water depth (Deuser and Hunt, 1969; Kroopnick, 1985). Indeed, by ~1.86 ‰ lower $\delta^{13}C$ values are recorded for *G. crassaformis* (mean: 0.46 ‰) than for *G. ruber* (mean: 2.32 ‰) (Jakob et al., 2016; this study) (Fig. 5c). In general, $\delta^{13}C$ values of *G. ruber* and *G. crassaformis* fluctuate between minima of 1.36 ‰ and 0 ‰ during glacials and maxima of 2.97 ‰ and 0.97 ‰ during interglacials, respectively (Jakob et al., 2016; this study) (Fig. 5c). It has been shown in a former study that the glacial-interglacial foraminiferal $\delta^{13}C$ pattern at Site 849 during iNHG is strongly controlled by the amount of primary productivity in the Southern Ocean, which is highest during interglacials (high $\delta^{13}C$) and lowest during glacials (low $\delta^{13}C$) (Jakob et al., 2016).

Mg/Ca values of *G. crassaformis* vary between 0.82 mmol/mol and 3.02 mmol/mol (this study), being on average 1.43 mmol/mol lower than Mg/Ca ratios of *G. ruber* from the same site and time interval (Jakob et al., 2017) (Fig. 5d). Temperatures reconstructed from *G. crassaformis* Mg/Ca values cover a range from 1.0 °C to 11.6 °C. Thus, sub-thermocline temperatures at Site 849 derived from *G. crassaformis* are on average 19 °C lower than sea-surface temperatures as reflected by *G. ruber* (~22–27 °C [Jakob et al., 2017]) (Fig. 5d).

5.4 Thermocline development in the Eastern Equatorial Pacific

5.4.1 Geochemical evidence

Variations in the vertical temperature gradient within the upper water column allow to effectively monitor shifts in thermocline depth with a small temperature difference between surface and thermocline waters indicating a deep thermocline and vice versa (e.g., Steph et al., 2009; Nürnberg et al., 2015). Absolute values of surface-to-thermocline temperature gradients can be reconstructed from the Mg/Ca-based temperature gradient derived from surface-dwelling (e.g., *G. ruber*) and thermocline-dwelling (e.g., *G. crassaformis*) species. In addition, the $\delta^{18}O$ gradient of the same species provides information on relative changes in the surface-to-thermocline temperature gradient since the effect of global ice volume and salinity (i.e., the two other main factors beside temperature that affect foraminiferal $\delta^{18}O$ [Ravelo and Hillaire-Marcel, 2007]) should be identical for planktic species from the same locality.

The $\delta^{18}O$ and Mg/Ca-based temperature gradients between *G. ruber* and *G. crassaformis* at Site 849 show no glacial-interglacial cyclicity (Fig. 6b), indicating that thermocline depth in the EEP was unaffected by varying glacial vs.

Clim. Past Discuss., https://doi.org/10.5194/cp-2017-151
Manuscript under review for journal Clim. Past
Discussion started: 20 November 2017

interglacial climatic conditions. This observation is in line with previous model- (Lee and Poulsen, 2005) and proxy-based studies (Bolton et al., 2010; Jakob et al., 2017).

On longer time scales, the $\delta^{18}O$ gradient decreased by ~1 ‰ from ~2.64 Ma to 2.55 Ma (MIS G2–101), and remained relatively constant throughout the remainder of our study interval (~2.55–2.38 Ma; MIS 101–95) (Fig. 6b). The Mg/Ca-based temperature gradient shows the same overall pattern as the $\delta^{18}O$ gradient (i.e., a ~5 °C increase from ~2.64 Ma to 2.55 Ma, and a constant value of ~20 °C from ~2.55 to 2.38 Ma) (Fig. 6b). We interpret the decrease in the $\delta^{18}O$ gradient and the increase in the Mg/Ca-based temperature gradient from ~2.64 Ma to 2.55 Ma to represent a shoaling of the thermocline. From that time onwards, constant $\delta^{18}O$ and Mg/Ca-based temperature gradients suggest that the thermocline remained relatively shallow throughout the final phase of the late Pliocene/early Pleistocene iNHG until ~2.38 Ma.

5.4.2 Faunal and sedimentological evidence

Based on our data, the overall abundances of the deep-thermocline-dwelling species *G. crassaformis* at Site 849 were relatively low when the thermocline in the EEP was relatively deep (i.e., prior to ~2.55 Ma as indicated by the $\delta^{18}O$ and Mg/Ca-based temperature gradients) (Fig. 6c). More specifically, *G. crassaformis* was present in substantially reduced numbers only or even completely absent between ~2.73 and 2.64 Ma (MIS G7–G2) (with the exception of MIS G4 [~2.68–2.69 Ma]). Since ~2.64 Ma, i.e., when the thermocline started to shoal, relative *G. crassaformis* abundances increased markedly from typically <5 % to ~10–35 % such that representatives of this taxon are present continuously throughout the remainder of the study interval. The increase of *G. crassaformis* abundances occurs at the expense of the intermediate-thermocline-dwelling species *G. menardii* and *G. tumida*, which decline from ~30–75 % to only ~5–65 % (Fig. 6c). This observation suggests that prior to the final phase of the late Pliocene/early Pleistocene iNHG, when the thermocline was relatively deep, the living conditions for the deep-thermocline-dwelling species *G. crassaformis* were unfavorable. At the same time, low *G. crassaformis* abundances allowed intermediate-thermocline-dwelling species (such as *G. menardii* and *G. tumida*) to dominate the planktic foraminiferal assemblages.

In general, *G. crassaformis* reaches highest abundances in oxygen-depleted waters (Jones, 1967; Kemle von Mücke and Hemleben, 1999), while other environmental factors including temperature, salinity or nutrient availability are markedly less important (Cléroux et al., 2013). The oxygen content of deep waters (and accordingly the abundance of *G. crassaformis*) is typically closely coupled to surface-water productivity (with a lower oxygen level and higher *G. crassaformis* abundances in deeper waters when surface-water productivity is high) (Wilson et al., 2017). We therefore hypothesize that primary productivity at Site 849 prior to ~2.64 Ma (MIS G2) was relatively low (with the exception of MIS G4). Low primary productivity led to a reduction of organic matter remineralization and therefore oxygen consumption in deeper waters. An elevated oxygen content in deeper waters implies, in turn, low *G. crassaformis* abundances. Such a scenario is supported by the SAR-based primary productivity record from Site 849 (Jakob et al., 2016; this study), which clearly indicates low productivity rates prior to ~2.64 Ma when the thermocline was relatively deep compared to after ~2.64 Ma when the thermocline became shallow (Fig. 6b, d).

Clim. Past Discuss., https://doi.org/10.5194/cp-2017-151
Manuscript under review for journal Clim. Past
Discussion started: 20 November 2017

As outlined above, on longer timescales primary productivity at Site 849 appears to be coupled to variations in thermocline depth. The observed long-term trend in primary productivity is overprinted by a clear glacial-interglacial cyclicity particularly during the final phase of iNHG (MIS 100–96); the position of the thermocline, however, remained constant along the obliquity (i.e., 41-kyr) band (Fig. 6b, d). Notably, the accumulation rates of *G. crassaformis, G. menardii* and *G. tumida* perfectly capture the pattern derived by the SAR-based productivity record (Fig. 6c, d). This suggests that the abundances of deep- and intermediate-thermocline-dwelling foraminiferal species are coupled to the strength of the biological pump and can be used as a tracer for primary productivity at Site 849.

The relatively high $\delta^{13}C$ gradient for MIS G4–G2 as it emerges from our data (Fig. 6d) confirms the interpretation of Jakob et al. (2016) for MIS G1–95 that low-amplitude productivity changes prior to MIS 100 were mainly driven by the nutrient content within the upwelled water mass as long as the thermocline was relatively deep (as reflected by a low thermocline-to-surface temperature gradient prior to ~2.55 Ma [MIS 101]; Fig. 6b, d). High-amplitude productivity changes resulting from upwelling intensification played an important role from MIS 100 onward (Jakob et al., 2016). At the same time, the thermocline became relatively shallow (as reflected by a large thermocline-to-surface temperature gradient since ~2.55 Ma [MIS 101] at Site 849; Fig. 6b, d). This is unlikely a coincidence, but rather suggests that the thermocline depth reached a critical threshold at that time. Prior to this, relatively warm and nutrient-poor waters from above the thermocline have upwelled in the EEP. Consequently, primary productivity rates were low. When the thermocline became shallow enough, however, trade winds could deliver cooler, nutrient-enriched waters from below the thermocline to the surface, which allowed primary productivity to increase. Such a scenario is supported by the observation that lower SSTs prevailed at Site 849 during glacials since MIS 100 (Jakob et al., 2017) (Fig. 5d).

Our findings imply a marked effect of long-term thermocline state change on primary productivity in the EEP. In particular, when thermocline shoaling reached a critical threshold, primary productivity increased, thereby removing CO_2 from the surface ocean. Considering that the EEP contributes substantially to global biological production in the present-day oceans, the observed coupling between thermocline state change and primary productivity is of major importance for the Earth's climate; thus, it may have favored the early development of large ice sheets in the Northern Hemisphere.

6 Conclusions

We integrate new with previously published foraminiferal-based geochemical and faunal records and with sedimentological data for ODP Site 849 (~2.75–2.4 Ma, MIS G7–95) to reconstruct changes in thermocline depth in the EEP during the late Pliocene/early Pleistocene iNHG. Our data document a shoaling of the thermocline at Site 849 from ~2.64 to 2.55 Ma, while it remained relatively shallow until ~2.38 Ma, implying that major changes in thermocline depth in the EEP occurred shortly before the final phase of the late Pliocene/early Pleistocene iNHG (i.e., prior to MIS 100–96). This finding, which is in line with former studies (Fedorov et al., 2006; Dekens et al., 2007), supports the hypothesis that (sub-)tropical thermocline shoaling was a precondition to allow the development of large ice sheets in the Northern Hemisphere (Cane and Molnar,

2001). At the same time, our new data contradict studies that have documented substantial shifts in thermocline depth in the EEP only prior to ~3.5 Ma (Wara et al., 2005; Steph et al., 2010; Ford et al., 2012). Our new records also suggest a low primary productivity during times of a relatively deep thermocline prior to ~2.64 Ma (MIS G2). In turn, the relatively shallow thermocline associated with low SSTs after ~2.55 Ma allowed primary productivity to increase during prominent iNHG glacials (MIS 100–96).

Data availability

All data reported will be made available upon publication of this paper via the open access PANGAEA database (www.pangaea.de).

Author contributions

The project was designed by OF, KAJ, and JP. KAJ and CS carried out Mg/Ca analyses; JF and KAJ performed stable-isotope analyses. KAJ wrote the manuscript with input from all co-authors.

Competing interests

The authors declare that they have no conflict of interest.

Acknowledgments

Richard Norris (Scripps Institution of Oceanography, San Diego) provided invaluable support in foraminiferal taxonomy. Sven Hofmann (Goethe-University Frankfurt) and Silvia Rheinberger are thanked for stable-isotope and Mg/Ca analyses, respectively. André Bahr provided support in Mg/Ca sample preparation. Hans-Peter Meyer and Alexander Varychev (Heidelberg University) provided SEM assistance. Jani L. Biber, Verena Braun, Jakob Gänzler, Barbara Hennrich, Karsten Kähler, and Tobias Syla helped with processing of sediment samples. This research used samples provided by the Ocean Drilling Program, which was sponsored by the U.S. National Science Foundation and participating countries under the management of Joint Oceanographic Institutions, Inc. Funding for this study was provided by the German Research Foundation (DFG; grants FR2544/6 to O.F. and PR651/15 to J.P.).

References

Adelseck, C. G. and Anderson, T. F.: The late Pleistocene record of productivity fluctuations in the eastern equatorial Pacific Ocean, Geology, 6, 388–391, 1978.

Anand, P., Elderfield, H., and Conte, M. H.: Calibration of Mg/Ca thermometry in planktonic foraminifera from a sediment trap time series, Paleoceanography, 18, doi:1010.1029/2002PA000846, 2003.

Bailey, I., Hole, G. M., Foster, G. L., Wilson, P. A., Storey, C. D., Trueman, C. N., and Raymo, M. E.: An alternative suggestion for the Pliocene onset of major northern hemisphere glaciation based on the geochemical provenance of North Atlantic Ocean ice-rafted debris, Quaternary Sci. Rev., 75, 181–194, 2013.

Barker, S., Greaves, M., and Elderfield, H.: A study of cleaning procedures used for foraminiferal Mg/Ca paleothermometry, Geochem. Geophys. Geosys., 4, doi:10.1029/2003GC000559, 2003.

Bartoli, G., Sarnthein, M., and Weinelt, M.: Late Pliocene millennial-scale climate variability in the northern North Atlantic prior to and after the onset of Northern Hemisphere glaciation, Paleoceanography, 21, PA4205, doi:4210.1029/2005PA001185, 2006.

Berger, W. H., Bonneau, M.-C., and Parker, F. L.: Foraminifera on the deep-sea floor: lysocline and dissolution rate, Oceanol. Acta, 5, 249–258, 1982.

Bolton, C. T., Gibbs, S. J., and Wilson, P. A.: Evolution of nutricline dynamics in the equatorial Pacific during the late Pliocene, Paleoceanography, 25, PA1207, doi:1210.1029/2009PA001821, 2010.

Cane, M. A. and Molnar, P.: Closing of the Indonesian seaway as a precursor to east African aridification around 3–4 million years ago, Nature, 411, 157–162, 2001.

Cléroux, C., deMenocal, P., Arbuszewski, J., and Linsley, B.: Reconstructing the upper water column thermal structure in the Atlantic Ocean, Paleoceanography, 28, 503–516, 2013.

Dekens, P. S., Lea, D. W., Pak, D. K., Spero, H. J.: Core top calibration of Mg/Ca in tropical foraminifera: Refining paleotemperature estimation, Geochem. Geophys. Geosys., 3, doi:10.1029/2001GC000200, 2002.

Dekens, P. S., Ravelo, A. C., and McCarthy, M. D.: Warm upwelling regions in the Pliocene warm period, Paleoceanography, 22, PA3211, doi:3210.1029/2006PA001394, 2007.

Deuser, W. G. and Hunt, J. M.: Stable isotope ratios of dissolved inorganic carbon in the Atlantic, Deep-Sea Res., 16, 221–225, 1969.

Elderfield, H., Vautravers, M., and Cooper, M.: The relationship between shell size and Mg/Ca, Sr/Ca, $\delta^{18}O$, and $\delta^{13}C$ of species of planktonic foraminifera, Geochem. Geophys. Geosys., 3, doi:10.1029/2001GC000194, 2002.

Etourneau, J., Schneider, R., Blanz, T., and Martinez, P.: Intensification of the Walker and Hadley atmospheric circulations during the Pliocene-Pleistocene climate transition, Earth Planet. Sci. Lett., 297, 103–110, 2010.

Fairbanks, R. G., Sverdlove, M., Free, R., Wiebe, P., and Bé, W.: Vertical distribution and isotopic fractionation of living planktonic foraminifera from the Panama Basin, Nature, 298, 841–844, 1982.

Faul, K. L., Ravelo, A. C., and Delaney, M. L.: Reconstructions of upwelling, productivity, and photic zone depth in the eastern equatorial Pacific Ocean using planktonic foraminiferal stable isotopes and abundances, J. Foramin. Res., 30, doi:10.2113/0300110, 2000.

Fedorov, A. V. and Philander, S. G.: Is El Nino changing?, Science, 288, 1997–2002, 2000.

Fedorov, A. V., Pacanowski, R. C., Philander, S. G., and Boccaletti, G.: The effect of salinity on the wind-driven circulation and the thermal structure of the upper ocean, J. Phys. Oceanogr., 34, 1949–1966, 2004.

Fedorov, A. V., Dekens, P. S., McCarthy, M., Ravelo, A. C., deMenocal, P. B., Barriero, M., Pacanowski, R. C., and Philander, S. G.: The Pliocene paradox (mechanisms for a permanent El Niño), Science, 312, 1485–1489, 2006.

Ford, H. L., Ravelo, A. C., and Hovan, S.: A deep Eastern Equatorial Pacific thermocline during the early Pliocene warm period, Earth Planet. Sci. Lett., 355–356, 152–161, 2012.

Friedrich, O., Schiebel, R., Wilson, P. A., Weldeab, S., Beer, S. J., Cooper, M. J., and Fiebig, J.: Influence of test size, water depth, and ecology on Mg/Ca, Sr/Ca, $\delta^{18}O$ and $\delta^{13}C$ in nine modern species of planktic foraminifers, Earth Planet. Sci. Lett., 319, 133–145, 2012.

Greaves, M., Caillon, N., Rebaubier, H., Bartoli, G., Bohaty, S., Cacho, I., Clarke, L. J., Cooper, M., Daunt, C., Delaney, M., deMenocal, P., Dutton, A., Eggins, S., Elderfield, H., Garbe-Schoenberg, D., Goddard, E., Green, D., Groeneveld, J., Hastings, D., Hathorne, E., Kimoto, K., Klinkhammer, G., Labeyrie, L., Lea, D. W., Marchitto, T., Martinez-Boti, M. A., Mortyn, P. G., Ni, Y., Nuernberg, D., Paradis, G., Pena, L., Quinn, T., Rosenthal, Y., Russell, A., Sagawa, T., Sosdain, S., Stott, L., Tachikawa, K., Tappa, E., Thunell, R., Wilson, P. A.: Interlaboratory comparison study of calibration standards for foraminiferal Mg/Ca thermometry, Geochem. Geophys. Geosys., 9, Q08010, doi:08010.01029/02008GC001974, 2008

Jakob, K. A., Wilson, P. A., Bahr, A., Bolton, C. T., Pross, J., Fiebig, J., and Friedrich, O.: Plio-Pleistocene glacial-interglacial productivity changes in the eastern equatorial Pacific upwelling system, Paleoceanography, 31, 453–470, doi:410.1002/2015PA002899, 2016.

Jakob, K. A., Bolton, C. T., Wilson, P. A., Bahr, A., Pross, J., Fiebig, J., Kähler, K., Friedrich, O.: Glacial-interglacial changes in equatorial Pacific surface-water structure during the Plio-Pleistocene intensification of Northern Hemisphere Glaciation, Earth Planet. Sci. Lett., 463, 69–80, doi:10.1016/j.epsl.2017.1001.1028, 2017.

Jones, J. I.: Significance of distribution of planktonic foraminifers in the Equatorial Atlantic Undercurrent, Micropaleontology, 13, 489–501, 1967.

Kemle von Mücke, S. and Hemleben, C.: Foraminifera, in: South Atlantic Zooplankton, Vol. 1, edited by: Boltovskoy, D., Backhuys Publishers, Leiden, 43–74, 1999.

Koutavas, A. and Lynch-Stieglitz, J.: Glacial-interglacial dynamics of the eastern equatorial Pacific cold tongue-Intertropical Convergence Zone system reconstructed from oxygen isotope records, Paleoceanography, 18, doi:1010.1029/2003PA000894, 2003.

Kroopnick, P. M.: The distribution of ^{13}C of ΣCO_2 in the world oceans, Deep-Sea Res., 32, 57–84, 1985.

Lee, S. Y. and Poulsen, C. J.: Tropical Pacific climate response to obliquity forcing in the Pleistocene, Paleoceanography, 20, PA4010, doi:4010.1029/2005PA001161, 2005.

Lin, H.-L., Peterson, L. C., Overpeck, J. T., Trumbore, S. E., and Murray, D. W.: Late Quaternary climate change from $\delta^{18}O$ records of multiple species of planktonic foraminifera: High-resolution records from the Anoxic Cariaco Basin, Venezuela, Paleoceanography, 12, 415–427, 1997.

Lisiecki, L. E. and Raymo, M. E.: A Pliocene-Pleistocene stack of 57 globally distributed benthic $\delta^{18}O$ records, Paleoceanography, 20, PA1003, doi:1010.1029/2004PA001071, 2005.

Locarnini, R. A., Mishonov, A. V., Antonov, J. I., Boyer, T. P., Garcia, H. E., Baranova, O. K., Zweng, M. M., Paver, C. R., Reagan, J. R., Johnson, D. R., Hamilton, M., and Seidov, D.: World Ocean Atlas 2013, Volume 1, Temperature, in: NOAA Atlas NESDIS 73, edited by: Levitus, S. and Mishonov, A., U. S. Government Printing Office, Washington, D. C., 40 pp, 2013.

Ma, H., Wu, L., and Li, Z.: Impact of freshening over the Southern Ocean on ENSO, Atmos. Sci. Lett., 14, 28–33, doi:10.1002/asl1002.1410, 2013.

Mayer, L., Pisias, N., and Janecek, T. et al.: Proc. ODP, Init. Repts., 138, College Station, TX, Ocean Drilling Program, 1992.

Mix, A. C., Pisias, N. G., Rugh, W., Wilson, J., Morey, A., and Hagelberg, T. K.: Benthic foraminifer stable isotope record from Site 849 (0–5 Ma): local and global climate changes, in: Proc. ODP, Sci. Results, 138, College Station, TX (Ocean Drilling Program), edited by: Pisias, N. G., Mayer, L. A., Janecek, T. R., Palmer-Julson, A., and van Adel, T. H., 371–412, 1995.

Mudelsee, M. and Raymo, M. E.: Slow dynamics of the Northern Hemisphere Glaciation, Paleoceanography, 20, PA4022, doi:4010.1029/2005PA001153, 2005.

Naafs, B. D. A., Hefter, J., and Stein, R.: Millennial-scale ice rafting events and Hudson Strait Heinrich(-like) Events during the late Pliocene and Pleistocene: a review, Quaternary Sci. Rev., 80, 1–28, 2013.

Niebler, H.-S., Hubberten, H.-W., and Gersonde, R.: Oxygen isotope values of planktic foraminifera: A tool for the reconstruction of surface water stratification, in: Use of Proxies in Paleoceanography, edited by: Fischer, G. and Wefer, G., Springer, New York, 165–189, 1999.

Nürnberg, D., Böschen, T., Doering, K., Mollier-Vogel, E., Raddatz, J., and Schneider, R.: Sea surface and subsurface circulation dynamics off equatorial Peru during the last ~17 kyr, Paleoceanography, 30, 984–999, doi:910.1002/2014pa002706, 2015.

Pennington, J. T., Mahoney, K. L., Kuwahara, V. S., Kolber, D. D., Calienes, R., and Chavez, F. P.: Primary production in the eastern tropical Pacific: A review, Prog. Oceanogr., 69, 285–317, 2006.

Ravelo, A. C. and Hillaire-Marcel, C.: The use of oxygen and carbon isotopes of foraminifera in Paleoceanography, in: Proxies in Late Cenozoic Paleoceanography, edited by: Hillaire-Marcel, C. and De Vernal, A., Elsevier, Amsterdam, Oxford, 735–764, 2007.

Regenberg, M., Steph, S., Nürnberg, D., Tiedemann, R., and Garbe-Schönberg, D.: Calibrating Mg/Ca ratios of multiple planktonic foraminiferal species with δ^{18}O-calcification temperatures: Paleothermometry for the upper water column, Earth Planet. Sci. Lett., 278, 324–336, 2009.

Schlitzer, R.: Export production in the equatorial and north Pacific derived from dissolved oxygen, nutrient and carbon data, J. Oceanogr., 60, 53–62, 2004.

Shackleton, N. J., Backman, J., Zimmerman, H., Kent, D. V., Hall, M., Roberts, D., Schnitker, D., Baldauf, J., Desprairies, A., and Homrighausen, R.: Oxygen isotope calibration of the onset of ice-rafting and history of glaciation in the North Atlantic region, Nature, 307, 620–623, 1984.

Spero, H. J., Mielke, K. M., Kalve, E. M., Lea, D. W., and Pak, D. K.: Multispecies approach to reconstructing eastern equatorial Pacific thermocline hydrography during the past 360 kyr, Paleoceanography, 18, doi:10.1029/2002PA000814, 2003.

Steph, S., Tiedemann, R., Prange, M., Groeneveld, J., Nürnberg, D., Reuning, L., Schulz, M., and Haug, G. H.: Changes in Caribbean surface hydrography during the Pliocene shoaling of the Central American Seaway, Paleoceanography, 21, PA4221, doi:4210.1029/2004PA001092, 2006.

Steph, S., Regenberg, M., Tiedemann, R., Mulitza, S., and Nürnberg, D.: Stable isotopes of planktonic foraminifera from tropical Atlantic/Caribbean core-tops: Implications for reconstructing upper ocean stratification, Mar. Micropaleontol., 71, 1–19, doi:10.1016/j.marmicro.2008.1012.1004, 2009.

Steph, S., Tiedemann, R., Prange, M., Groeneveld, J., Schulz, M., Timmermann, A., Nürnberg, D., Rühlemann, C., Saukel, C., and Haug, G. H.: Early Pliocene increase in thermohaline overturning: A precondition for the development of the modern equatorial Pacific cold tongue, Paleoceanography, 25, PA2202, doi:2210.1029/2008PA001645, 2010.

Takahashi, T., Sutherland, S. C., Wanninkhof, R., Sweeney, C., Feely, R. A., Chipman, D. W., Hales, B., Friederich, G., Chavez, F., Sabine, C., Watson, A., Bakker, D. C. E., Schuster, U., Metzl, N., Yoshikawa-Inoue, H., Ishii, M., Midorikawa, T., Nojiri, Y., Körtzinger, A., Steinhoff, T., Hoppema, M., Olafsson, J., Arnarson, T. S., Tilbrook, B., Johannessen, T., Olsen, A., Bellerby, R., Wong, C. S., Delille, B., Bates, N. R., de Baar, H. J. W.: Climatological mean and decadal change in surface ocean pCO_2, and net sea-air CO_2 flux over the global oceans, Deep-Sea Res. Pt II, 56, 554–577, 2009.

Tedesco, K., Thunell, R., Astor, Y., and Muller-Karger, F.: The oxygen isotope composition of planktonic foraminifera from the Cariaco Basin, Venezuela: Seasonal and interannual variations, Mar. Micropaleontol., 62, 180–193, 2007.

Toggweiler, J. R. and Sarmiento, J. L.: Glacial to interglacial changes in atmospheric carbon dioxide: the critical role of ocean surface water in high latitudes, in: The carbon cycle and atmospheric CO_2: Natural variations Archean to present, edited by: Sundquist, E. T. and Broecker, W. S., Geoph. Monog. Series 32, American Geophysical Union, Washington, D. C., 163–184, 1985.

Wang, B., Wu, R., and Lukas, R.: Annual adjustment of the thermocline in the tropical Pacific Ocean, J. Climate, 13, 596–616, 2000.

Wara, M. W., Ravelo, A. C., and Delaney, M. L.: Permanent El Niño-like conditions during the Pliocene warm period, Science, 309, 758–761, 2005.

Watkins, J. M., Mix, A. C., and Wilson, J.: Living planktic foraminifera in the central tropical Pacific Ocean: Articulating the equatorial "cold tongue" during La Niña, Mar. Micropaleontol., 33, 157–174, 1998.

Wejnert, K. E., Thunell, R. C., and Margarita Astor, Y.: Comparison of species-specific oxygen isotope paleotemperature equations: Sensitivity analysis using planktonic foraminifera from the Cariaco Basin, Venezuela, Mar. Micropaleontol., 101, 76–88, 2013.

Wilson, J., Abboud, S., and Beman, J. M.: Primary production, community respiration, and net community production along oxygen and nutrient gradients: Environmental controls and biogeochemical feedbacks within and across "Marine Lakes", Front. Mar. Sci., 4, doi:10.3389/fmars.2017.00012, 2017.

Wyrtki, K.: An estimate of equatorial upwelling in the Pacific, J. Phys. Oceanogr., 11, 1205–1214, 1981.

Clim. Past Discuss., https://doi.org/10.5194/cp-2017-151
Manuscript under review for journal Clim. Past
Discussion started: 20 November 2017

Climate of the Past Discussions
Open Access
EGU

Table 1: Compilation of the geochemical datasets from ODP Site 849 evaluated in this study.

Foraminiferal species	Size fraction	Proxy	Interval	Reference
G. crassaformis (sinistral- and dextral-coiling)	315–400 µm	$\delta^{13}C$	74.17–67.78 mcd (~2.65–2.4 Ma; MIS G1–95)	Jakob et al. (2016)
			77.02–74.19 mcd (~2.75–2.65 Ma; MIS G7–G2)	this study
	315–400 µm	$\delta^{18}O$	77.02–67.78 mcd (~2.75–2.4 Ma; MIS G7–95)	this study
	315–400 µm	Mg/Ca	77.02–67.78 mcd (~2.75–2.4 Ma; MIS G7–95)	this study
G. ruber (white, sensu stricto)	250–315 µm	$\delta^{13}C$	74.17–67.78 mcd (~2.65–2.4 Ma; MIS G1–95)	Jakob et al. (2016)
			77.02–74.19 mcd (~2.75–2.65 Ma; MIS G7–G2)	this study
	250–315 µm	$\delta^{18}O$	77.02–67.78 mcd (~2.75–2.4 Ma; MIS G7–95)	Jakob et al. (2017)
	200–250 µm	Mg/Ca	77.02–67.78 mcd (~2.75–2.4 Ma; MIS G7–95)	Jakob et al. (2017)

Clim. Past Discuss., https://doi.org/10.5194/cp-2017-151
Manuscript under review for journal Clim. Past
Discussion started: 20 November 2017

Climate of the Past Discussions
Open Access
EGU

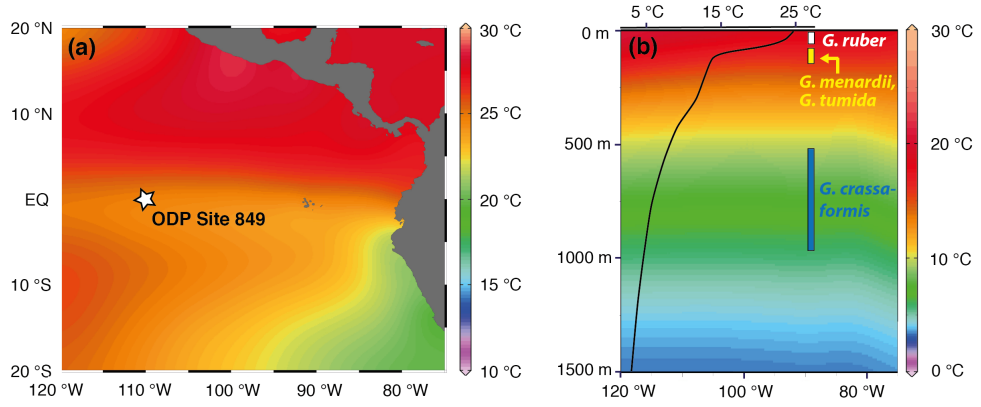

Figure 1: Location of study area within the Eastern Equatorial Pacific and present-day temperature profile at studied site. (a) Map showing the location of ODP Site 849 in the "EEP cold tongue". Colors denote mean annual surface-water temperatures. (b) Mean annual temperature profile for Site 849 showing the position of the thermocline. Calcification depths of foraminiferal species analyzed in this study are indicated by white (*G. ruber*), yellow (*G. menardii* and *G. tumida*) and blue (*G. crassaformis*) bars (see Sect. 3 for details). Maps are after World Ocean Atlas (Locarnini et al., 2013).

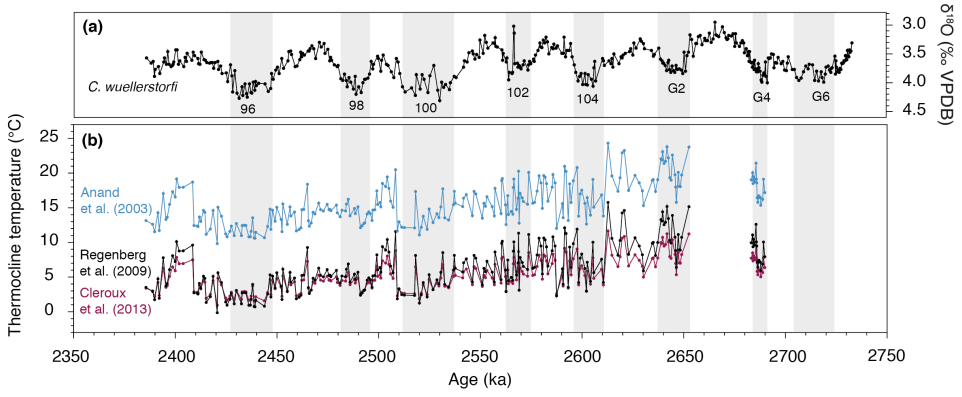

Figure 2: Species-specific conversions of Mg/Ca ratios to temperature for *G. crassaformis*. (a) Benthic foraminiferal (*C. wuellerstorfi*) $\delta^{18}O$ stratigraphy (Jakob et al., 2017). (b) Comparison of the different species-specific Mg/Ca to temperature conversions of Cléroux et al. (2013) (red), Regenberg et al. (2009) (black) and Anand et al. (2003) (blue) applied to *G. crassaformis* Mg/Ca values from Site 849 for ~2.75 to 2.4 Ma. Gaps in the dataset for 2.68–2.65 Ma (MIS G3) and 2.73–2.69 Ma (MIS G7–G5) are due to a lack of *G. crassaformis* specimens in the investigated (315–400 µm) size fraction.

Clim. Past Discuss., https://doi.org/10.5194/cp-2017-151
Manuscript under review for journal Clim. Past
Discussion started: 20 November 2017

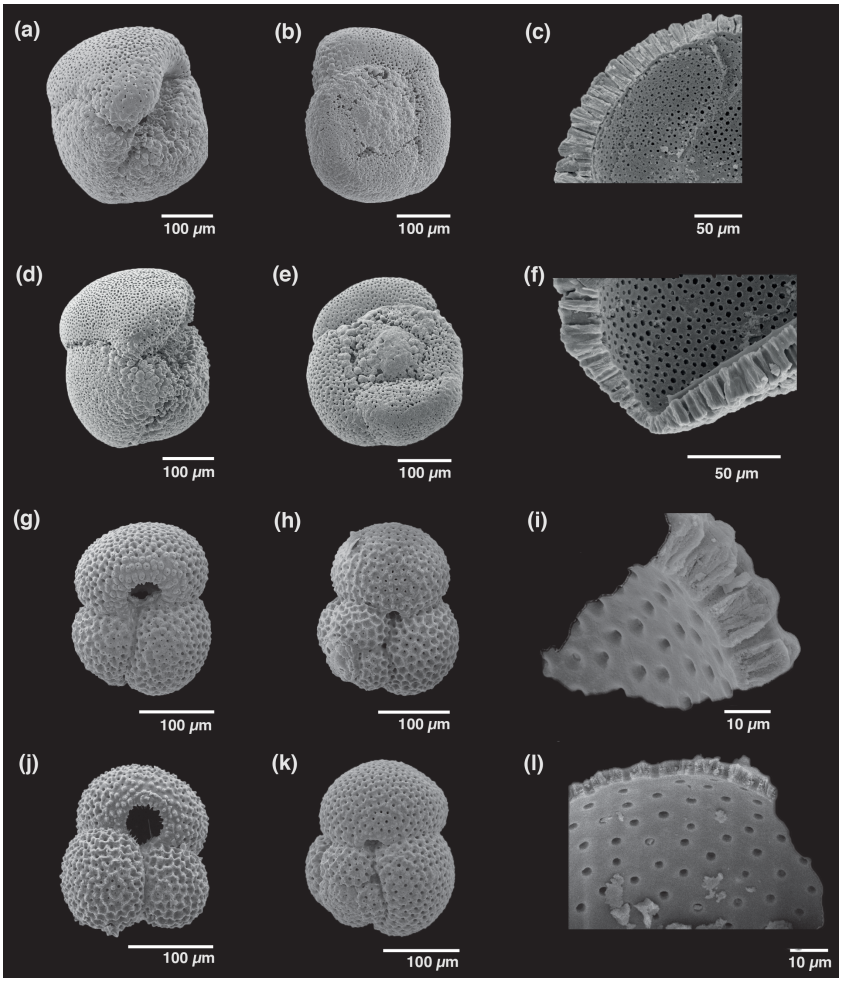

Figure 3: Scanning Electron Micrographs of *Globorotalia crassaformis* and *Globigerinoides ruber* from ODP Site 849. Both glacial (a–c, g–i) and interglacial (d–f, j–l) foraminiferal tests are well preserved, allowing for the acquisition of reliable geochemical data.

Clim. Past Discuss., https://doi.org/10.5194/cp-2017-151
Manuscript under review for journal Clim. Past
Discussion started: 20 November 2017

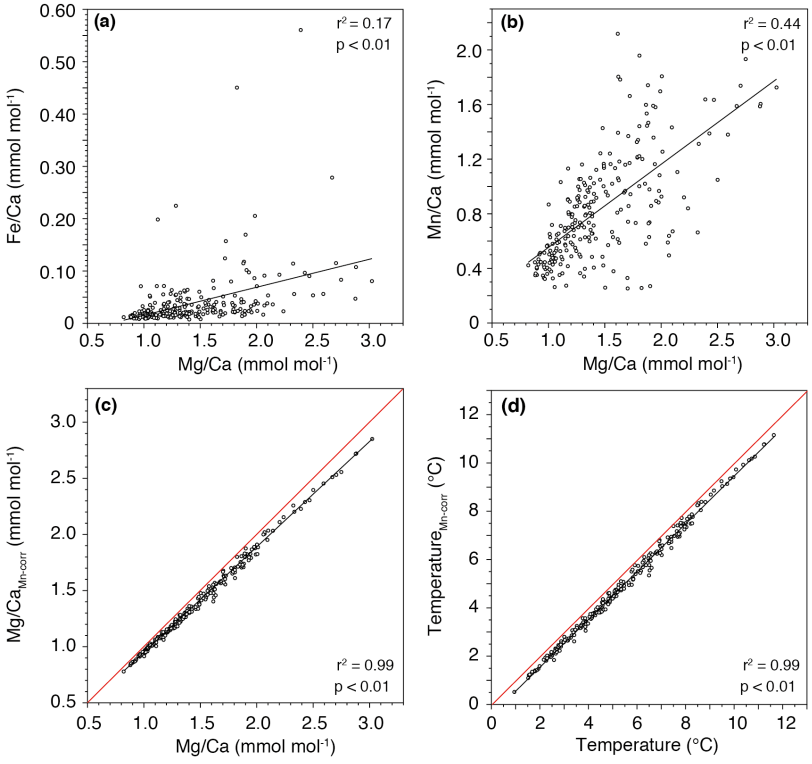

Figure 4: Evaluation of potential contamination on Mg/Ca ratios in *G. crassaformis*. (a) Cross plot between measured Mg/Ca and Fe/Ca ratios. (b) Cross plot between measured Mg/Ca and Mn/Ca ratios. (c) Cross plot between measured Mg/Ca and Mg/Ca ratios corrected for Mn-bearing overgrowths (using the assumption of an unrealistically high Mg/Mn ratio of 1) in comparison to uncontaminated samples (red line). (d) Cross plot between temperatures calculated from measured Mg/Ca and Mg/Ca ratios corrected for Mn-bearing overgrowths (using the assumption of an unrealistically high Mg/Mn ratio of 1) in comparison to uncontaminated samples (red line) (see Sect. 5.2 for details).

Clim. Past Discuss., https://doi.org/10.5194/cp-2017-151
Manuscript under review for journal Clim. Past
Discussion started: 20 November 2017

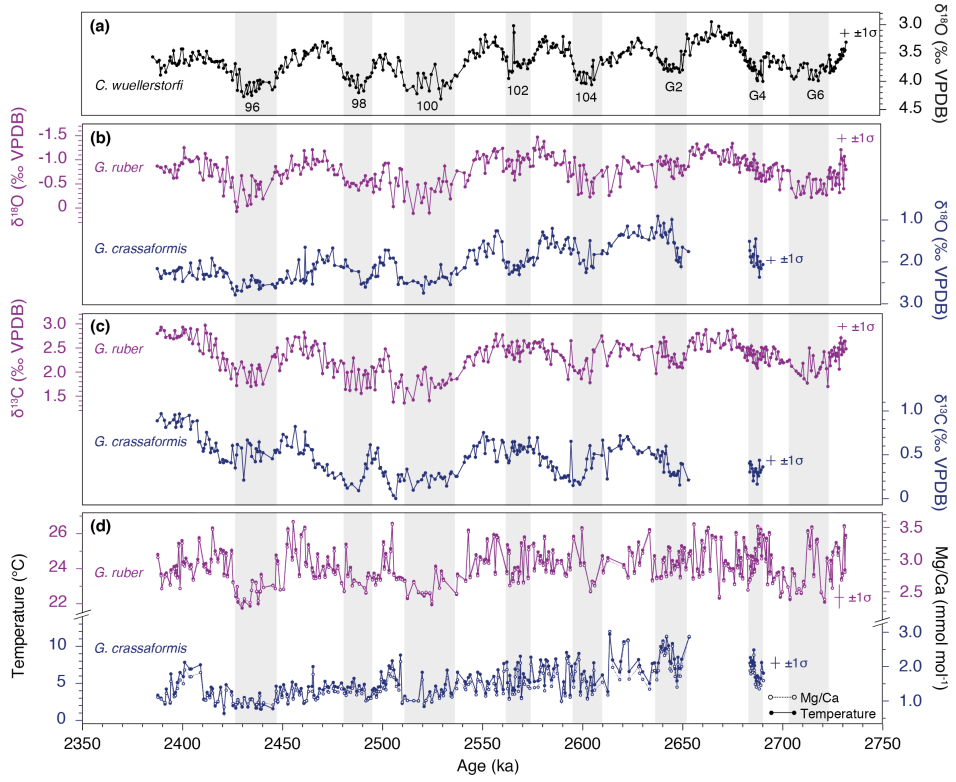

Figure 5: Planktic foraminiferal proxy records from ODP Site 849 for MIS G7–95 (~2.75–2.4 Ma). (a) Benthic foraminiferal (*C. wuellerstorfi*) $\delta^{18}O$ stratigraphy (Jakob et al., 2017). (b) $\delta^{18}O$ data of *G. ruber* (purple; Jakob et al. [2017]) and *G. crassaformis* (blue; this study). (c) $\delta^{13}C$ data of *G. ruber* (purple; Jakob et al. [2016], this study) and *G. crassaformis* (blue; Jakob et al. [2016], this study). (d) Mg/Ca (dashed line, open dots) and temperature (solid line, filled dotes) data of *G. ruber* (purple; Jakob et al. [2017]) and *G. crassaformis* (blue; this study). Gaps in the G. *crassaformis* dataset for 2.68–2.65 Ma (MIS G3) and 2.73–2.69 Ma (MIS G7–G5) are due to a lack of *G. crassaformis* specimens in the investigated (315–400 µm) size fraction. Horizontal and vertical bars indicate the 1σ standard deviation associated with the age model and the individual proxy records, respectively. Grey bars highlight glacial periods.

Clim. Past Discuss., https://doi.org/10.5194/cp-2017-151
Manuscript under review for journal Clim. Past
Discussion started: 20 November 2017

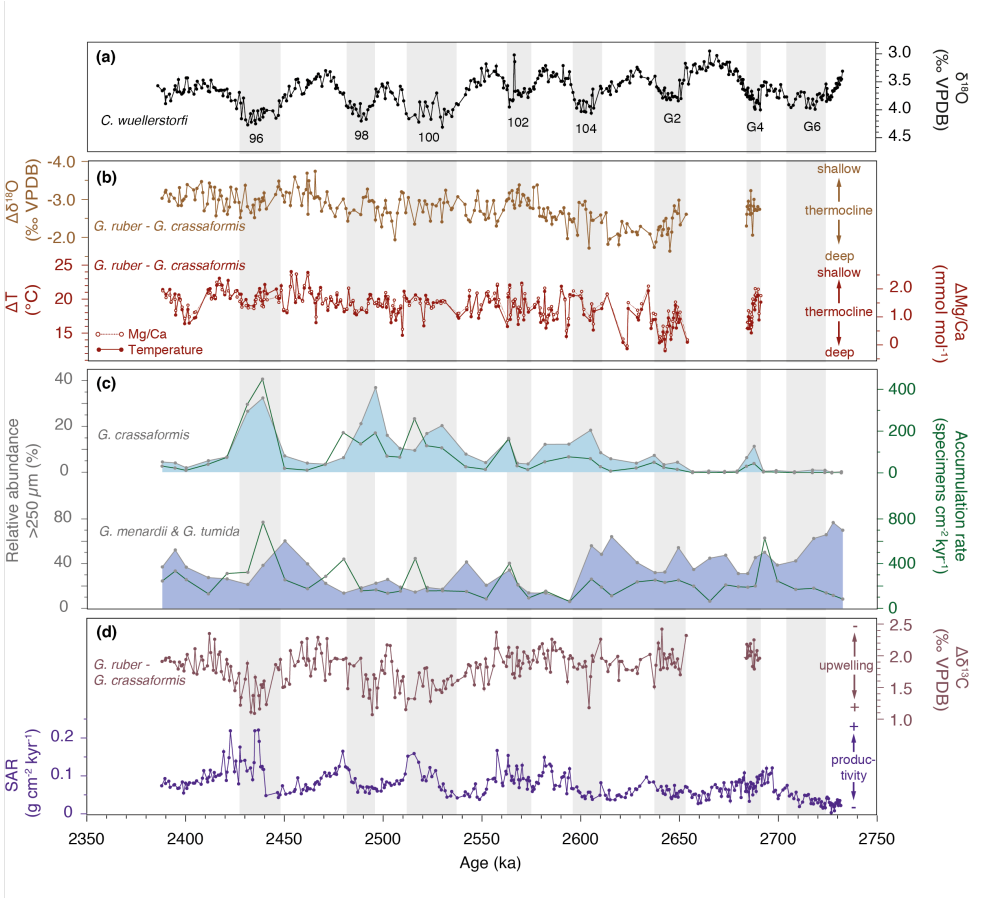

Figure 6: Compilation of planktic foraminiferal, faunal and sedimentary proxy records from ODP Site 849 for MIS G7–95 (~2.75–2.4 Ma). (a) Benthic foraminiferal (*C. wuellerstorfi*) $\delta^{18}O$ stratigraphy (Jakob et al., 2017). (b) $\delta^{18}O$ (brown; this study) and Mg/Ca (red dashed line with open dots; this study) and temperature (red; this study) gradients between the surface-dwelling species *G. ruber* and the thermocline-dwelling species *G. crassaformis* as a proxy for relative thermocline depth. (c) Relative abundances of *G. crassaformis* (light blue; this study) and *G. menardii* and *G. tumida* (dark blue; this study) together with their mass-accumulation rates (green; this study). (d) $\delta^{13}C$ gradient between *G. ruber* and *G. crassaformis* as an indicator for upwelling strength (purple; Jakob et al. [2016], this study) together with sand-accumulation rates as an indicator for primary productivity (Jakob et al. [2016], this study). Gaps in the $\delta^{18}O$, $\delta^{13}C$ and Mg/Ca gradients for 2.68–2.65 Ma (MIS G3) and 2.73–2.69 Ma (MIS G7–G5) are due to a lack of *G. crassaformis* specimens in the investigated (315–400 µm) size fraction.